ULTRASONIC IMAGING **24,** 1-12 (2002)

Tissue Motion and Elevational Speckle Decorrelation in Freehand 3D Ultrasound

PAI-CHI LI, CHENG-YEN LI AND WEN-CHUN YEH

Department of Electrical Engineering
National Taiwan University
Tapei, Taiwan, R.O.C.
paichi@cc.ee.ntu.edu.tw

3D positioning is essential for quantitative volume analysis in 3D ultrasound. Particularly for freehand scanning without an external positioning device, such information must be estimated by analyzing the original 2D images prior to 3D reconstruction. Previous work on freehand 3D positioning has focused on elevational displacement estimation using speckle decorrelation for linear scans. However, the effects of other types of motion have been ignored. Given that all types of motion potentially introduce speckle decorrelation, the accuracy of the elevational displacement estimation is likely to be diminished by the presence of motions of other types. In the present study, simulations were performed to probe the effects of various motions on elevational displacement estimation. In particular, the effects of rotational motions on image correlation are investigated in detail. It is found that these motions significantly affect the estimation results and thus should be taken into account when reconstructing the 3D image. In addition, speckle variations also affect the estimation even when only elevational motion is present. Finally, full motion analysis in freehand scanning may not be possible by only using speckle correlation analysis unless speckle variations can be reduced and the correlation distribution under complex motion can be obtained.

KEY WORDS: 3D ultrasound; elevational decorrelation; motion analysis; speckle correlation; speckle tracking.

I. INTRODUCTION

Over the last few years, tremendous progress has been made in the field of 3D ultrasound due to the application of advanced computer technologies.[1] 3D imaging permits 3D representation of anatomical structures by displaying the entire volume in a single image. Central to 3D ultrasound is the reconstruction of a 3D image from a set of 2D images. The accuracy of this volume reconstruction depends on the accuracy with which the 3D positioning is determined. If a fully-sampled 2D array is used, 2D steering and 3D focusing can be performed and, hence, the volume data can be directly acquired with accurate positioning information.[2] Such an approach is very complex, however, and must be simplified to be of practical use. The simplification of this approach leads to final images of suboptimal quality. For conventional systems using 1D transducer arrays, on the other hand, 3D volume data is reconstructed from a set of two images with the aid of information from an external positioning device. Most positioning techniques require a supplementary device to record the location of the transducer during scanning. This device may be mechanical or magnetic. Clinical applications of such 3D imaging methods have been limited due to the need for an external positioning device and the fact that reconstruction is not real-time.

Freehand scanning without a positioning device has also been proposed for systems using 1D arrays.[3-7] Commercial products are also available that allow an operator to manually translate an ultrasound probe across a patient target. A 3D ultrasound image volume is then derived from correlated frames of ultrasound image data.[8] In this method, the transducer is

0161-7346/02 $18.00

linearly moved along the elevational direction while 2D images are being acquired. The resulting set of 2D images is then used to reconstruct 3D volume data. Elevational speckle decorrelation is typically used to estimate the displacement in elevation.[4] This technique is based on the fact that the correlation between two consecutive images acquired during linear scanning is determined by the elevational displacement relative to the elevational beam width. Such elevational speckle decorrelation has also been extended to a fan type scanning by acquiring depth-dependent elevational displacement information.[7] One limitation of this approach is that it is restricted to simple motion only (i.e., only one type of motion). For general freehand scanning, more complex motion (i.e., more than one type of motion) may be present and the decorrelation between successive images is affected. In this case, the elevational displacement is overestimated because the speckle decorrelation from other motions is also included. The elucidation of such effects requires a thorough correlation analysis of systems where complex probe-to-tissue motion is present. The primary purpose of this paper is to use computer simulations to study the effects of complex motion on image correlation/decorrelation. The feasibility and limitations of applying the correlation technique to full motion analysis are discussed.

The paper is organized as follows. In section II, an overview of the fundamentals of elevational speckle decorrelation is given and a computer simulation model is described. Decorrelation due to complex tissue motion is investigated in section III and its effects on elevational motion estimation are studied in section IV. The paper concludes in section V with a discussion on the feasibility and limitations of full motion analysis using the correlation-based approach.

II. SIMULATION MODEL

For fully-developed speckle (i.e., a homogeneous distribution of scatterers with a uniform scattering strength and uncorrelated microscopic structures), the correlation as a function of tissue motion can be derived.[9] Assuming a linear imaging process with a space invariant point spread function (PSF), a received echo can be represented as the convolution of the PSF and the scatterer distribution function. Let $a(\bullet)$ be the scatterer distribution function and $b(\bullet)$ be the PSF. Then, the received signal $s(\bullet)$ is

$$s(u) = \int_{-\infty}^{\infty} a(u')b(u-u')du' \tag{1}$$

where a 3D coordinate system denoted by $u = (x, y, z)$ is used. The complex cross-correlation function $c(u_1,u_2)$ of two received echoes $s_1(u_1)$ and $s_2(u_2)$ is

$$c(u_1,u_2) \equiv < s_1(u_1)s_2^{*}(u_2) > = \int\int_{-\infty}^{\infty} < a(u')a^{*}(u''-u_0) > b(u_1-u')b^{*}(u_2-u'')du'du'' \tag{2}$$

where $< \bullet >$ represents the ensemble average and u_0 is the 3D scatterer displacement between the two measurements. Since the insonified region is fully developed speckle, we have

$$< a(u')a^{*}(u''-u_0) > = a_0{}^2\delta(u'-u''+u_0) \tag{3}$$

where $\delta(\bullet)$ is the 3D Dirac-delta function and a_0 is the scattering strength. Hence, Eq. (2) can be rewritten as

$$c(u_1,u_2) = {a_0}^2 \int_{-\infty}^{\infty} b(u_1 - u')b^*(u_2 - u' - u_0)du' \tag{4}$$

When the cross-correlation function is evaluated at $u_1 = u_2$, Eq. (4) becomes

$$c(u_1,u_1) = {a_0}^2 \int_{-\infty}^{\infty} b(u_1 - u')b(u_1 - u' - u_0)du' = {a_0}^2 \int_{-\infty}^{\infty} b(u''')b(u''' - u_0)du''' \tag{5}$$

The above equation shows that the correlation between two signals from the same sample volume can be represented by the autocorrelation function of the PSF of the system.[9] Nonetheless, the above equations consider only scatterer translation; the effects of rotation are not included.

Simulations were carried out to analyze the correlation distribution between two 2D images with relative motion. The model described by Li and Chen was adopted for the simulations.[10] The PSF described in Eq. (1) is a separable, cosine-modulated 3D Gaussian function expressed as follows

$$b(u) \equiv b(x,y,z) = e^{-\pi\left(\frac{x^2}{\sigma_x^2}+\frac{y^2}{\sigma_y^2}+\frac{z^2}{\sigma_z^2}\right)} \cos(2\pi f_0 z) \tag{6}$$

where x, y, and z denote the lateral, elevational and axial directions respectively. In the simulations, the center frequency f_0 was at 5 MHz, and σ_x, σ_y and σ_z were the –6.82 dB widths of the PSF in the three respective directions (assigned a value of $\sigma_x = \sigma_y = \sigma_z = 0.3$ mm). To obtain a 2D B-mode image, the envelope of the predetection signal is computed at a fixed elevational position (e.g., $y = y_0$). Envelope detection was carried out using the Hilbert transform. The scatterer distribution function defines randomly-distributed scatterers with uniformly-distributed random amplitudes on a 3D grid. In the simulations, a discrete model was used with a minimum spacing between two adjacent grid points of 0.02 mm. The total number of scatterers was 1/100 of the total available grid points. To avoid potential artifacts introduced by the discretization, the effects of motion on length scales shorter than the grid spacing were taken into account by modifying the phase of the corresponding scatterer.[11]

Using this model, 3D tissue motion was simulated by rotating and translating the original position of a scatterer (x_i, y_i, z_i) to a new position (x_i', y_i', z_i'). For example, the following equation can be used to represent a rotation of angle α in the (x,z)-plane in addition to a translation of (x_0, y_0, z_0).

$$\begin{pmatrix} x_i' \\ y_i' \\ z_i' \end{pmatrix} = \begin{pmatrix} \cos\alpha & 0 & -\sin\alpha \\ 0 & 1 & 0 \\ \sin\alpha & 0 & \cos\alpha \end{pmatrix} \begin{pmatrix} x_i \\ y_i \\ z_i \end{pmatrix} - \begin{pmatrix} x_0 \\ y_0 \\ z_0 \end{pmatrix} \tag{7}$$

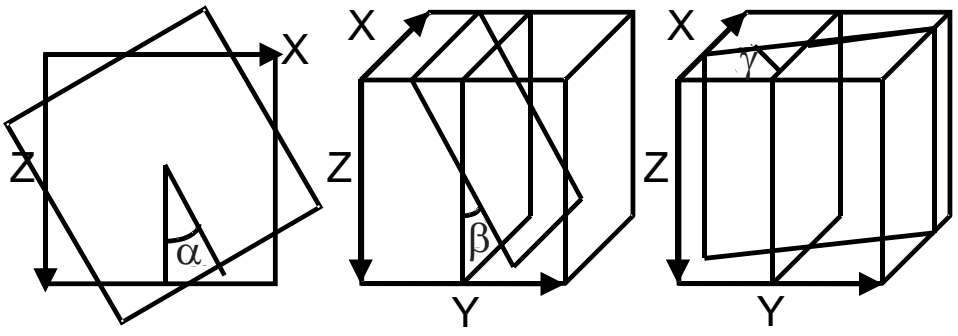

FIG. 1 Definition of the six motion parameters.

Likewise, rotation in the (y, z)-plane and the (x, y)-plane can be accomplished with the following equations:

$$\begin{pmatrix} x_i' \\ y_i' \\ z_i' \end{pmatrix} = \begin{pmatrix} 1 & 0 & 0 \\ 0 & \cos\beta & -\sin\beta \\ 0 & \sin\beta & \cos\beta \end{pmatrix} \begin{pmatrix} x_i \\ y_i \\ z_i \end{pmatrix} - \begin{pmatrix} x_0 \\ y_0 \\ z_0 \end{pmatrix} \tag{8}$$

$$\begin{pmatrix} x_i' \\ y_i' \\ z_i' \end{pmatrix} = \begin{pmatrix} \cos\gamma & -\sin\gamma & 0 \\ \sin\gamma & \cos\gamma & 0 \\ 0 & 0 & 1 \end{pmatrix} \begin{pmatrix} x_i \\ y_i \\ z_i \end{pmatrix} - \begin{pmatrix} x_0 \\ y_0 \\ z_0 \end{pmatrix} \tag{9}$$

III. CORRELATION ANALYSIS

As defined in figure 1, the scatterer can undergo a total of six types of motion denoted by $(x, y, z, \alpha, \beta, \gamma)$. In general, the in-plane motion (i.e., x, z and α) can be accurately estimated using speckle tracking.[12] Furthermore, speckle decorrelation due to x and z motion can be ignored when the motion is relatively small compared to the transmit depth of focus and aperture size.[13] Correlation changes due to the α motion (i.e., rotation in the 2D image plane), on the other hand, cannot be ignored. The reason for this is illustrated in the speckle images shown in figure 2. Fig. 2(a) shows a simulated speckle image and (b) shows the same image rotated clockwise by 4°. Rotation not only rotates the image but also changes the speckle characteristics. In other words, speckle decorrelation is introduced, which may affect other correlation-based motion estimations. The correlation distribution between the images in (a) and (b) is shown in (c), which indicates high correlation as white (0.90) and low correlation as black (0.66). The correlation coefficients shown in figure 2 and all the subsequent figures are calculated based on a tracked region sufficiently large (more than 10 independent speckle spots) to ensure reliable estimation results. At the center of the image, the decorrelation is only due to scatterer rotation. Upon moving away from the center, bulk translation is also present and hence the correlation diminishes. Figure 3 shows the correlation coefficient as a function of α at the center of rotation (i.e., without bulk translation). The

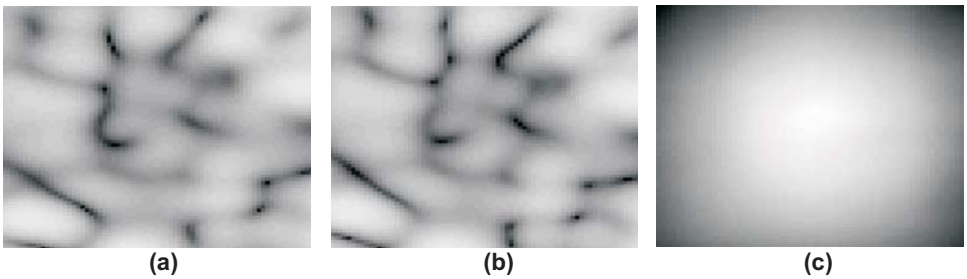

FIG. 2 (a) Speckle image before in-plane rotation. (b) Speckle image after in-plane rotation. (c) Correlation distribution (from 0.66 to 0.90).

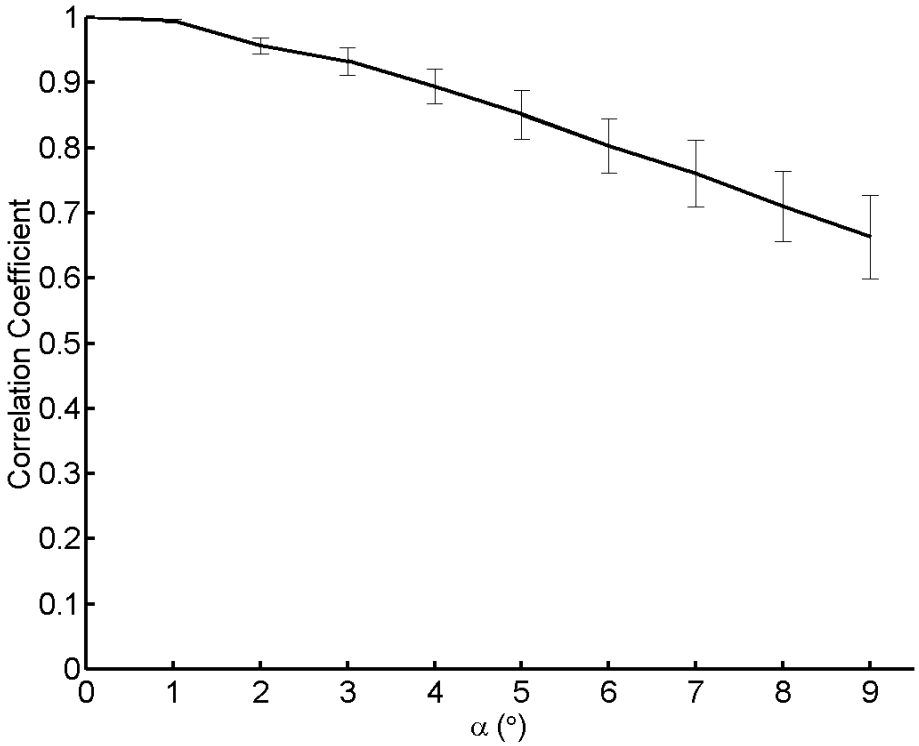

FIG. 3 Correlation coefficient as a function of in-plane rotation. Error bars represent +/- one standard deviation.

solid line represents the mean and the error bars indicate the +/- one standard deviation derived from 10 simulations with independent scatterer distributions.

The out-of-plane motion cannot be estimated by speckle tracking; however, such motion can be estimated from measurements of the speckle decorrelation. As shown in Eq. (5), the elevational (i.e., y) speckle decorrelation can be used to estimate the elevational motion if there is no rotation and the elevational beam is known. Figure 4 shows the speckle decorrelation (mean is depicted by the solid line and the error bars represent +/- one standard deviation) in comparison with the auto-correlation function of the elevational beam (dashed line). T he elevational beam has a –6.82 dB beam width of 0.4 mm. The two curves are similar, with minor differences at large displacements. The deviation at large displacements is due to the fact that the correlation is calculated using postdetection images instead of the complex data. In addition, small variations are present due to speckle variations as shown by

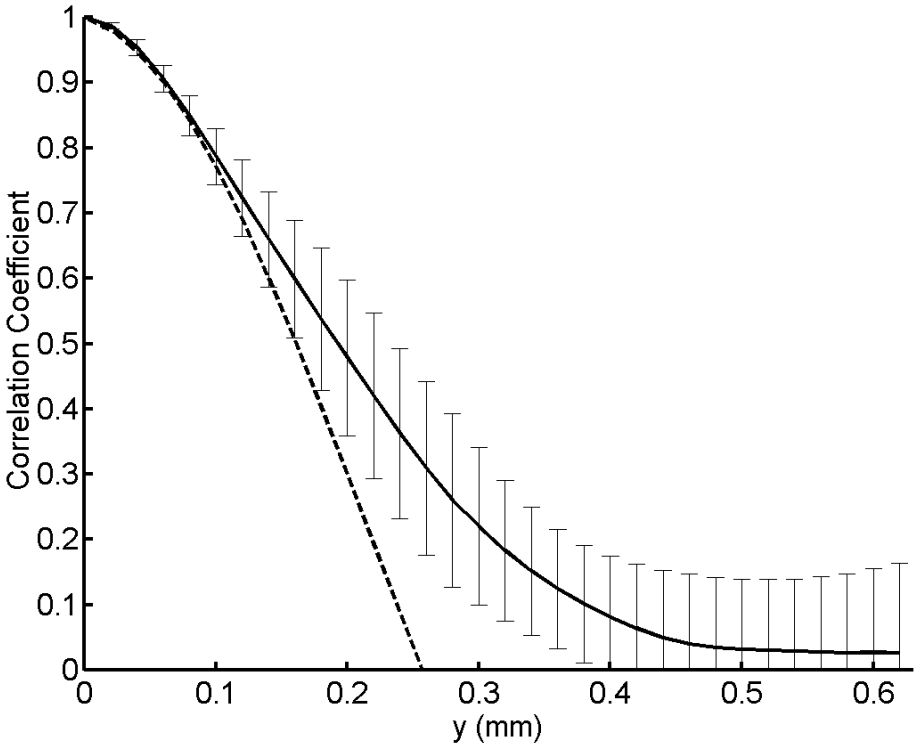

FIG. 4 Correlation coefficient as a function of elevational displacement. The solid line depicts the mean and the error bars show +/- one standard deviation of the correlation coefficient. The dashed line is the autocorrelation of the elevational beam.

the error bars.[9] This example therefore shows that it is possible to use the correlation between two images to estimate the elevational motion, but this estimation will be subject to errors due to the correlation variations. The above analysis is based on the fundamental assumption that only elevational motion is present. Thus, speckle decorrelation due to all other motions, including the three rotations, is ignored. Such an assumption is unlikely to be valid for freehand scanning.

The feasibility of using speckle correlation analysis to estimate the other out-of-plane motion parameters (i.e., β and γ) was also investigated. The β and γ motions result in decorrelation effects different from those observed for y motion. Figures 5 and 6 show the correlation distribution for β and γ, respectively. In each figure, the rotation is 4° and the center of rotation is at the center of the image. The horizontal axis is the lateral direction (x) and the vertical axis is the axial direction (z). The four panels in each figure depict: (a) a single realization of the scatterer distribution, (b) the averaged correlation from 5 independent realizations of the scatterer distribution, (c) the averaged correlation from 10 realizations, and (d) the averaged correlation from 20 realizations. The ranges of correlation coefficients are 0.85-0.92 for figure 5 and 0.92-0.98 for figure 6, where high correlation is indicated as white and low correlation is indicated as black. Significant errors are apparent in the panels with less averaging; such errors affect the accuracy of the estimation results. On the other hand, although averaging effectively reduces the variations, it cannot be implemented in practice because there is only one scatterer distribution available for a given imaging condition. Also note that the middle depth in figure 6 corresponds to the elevational focal point. Thus, the elevational beam is the narrowest at this depth and the correlation decreases more rapidly.

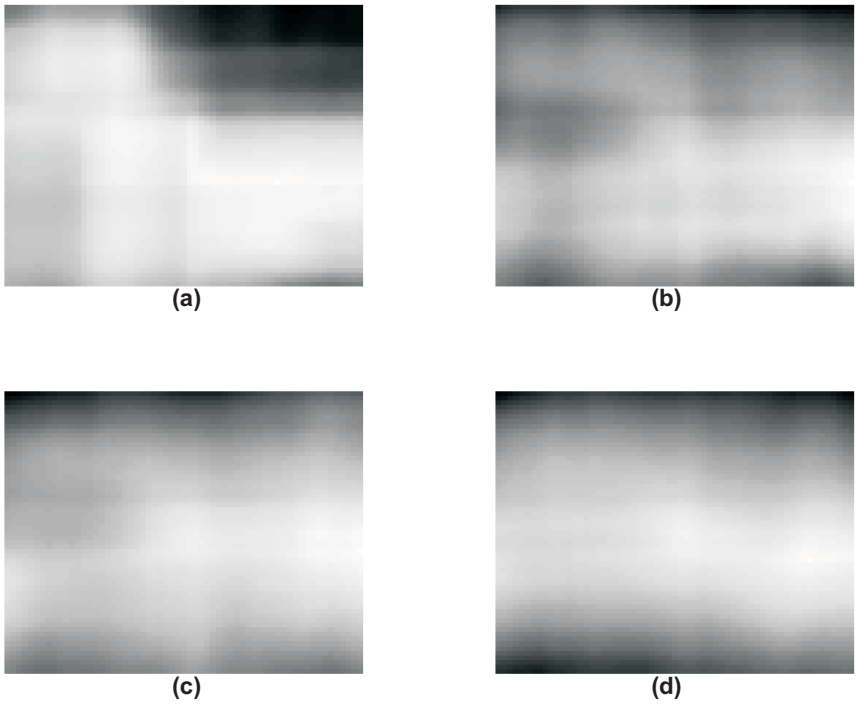

FIG. 5 Correlation distribution with a rotation in the *y*-*z* plane (i.e., β). (a) One realization; (b) average of 5 realizations; (c) average of 10 realizations; and (d) average of 20 realizations. The correlation coefficients range from 0.85 (black) to 0.92 (white).

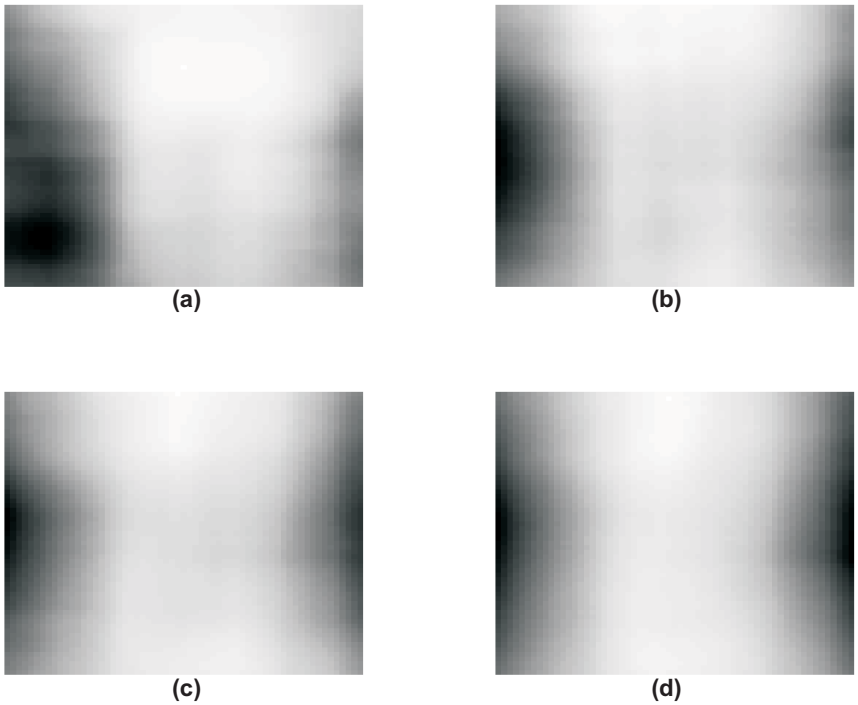

FIG. 6 Correlation distribution with a rotation in the *x*-*y* plane (i.e., γ). (a) One realization; (b) average of 5 realizations; (c) average of 10 realizations; and (d) average of 20 realizations. The correlation coefficients range from 0.92 (black) to 0.98 (white).

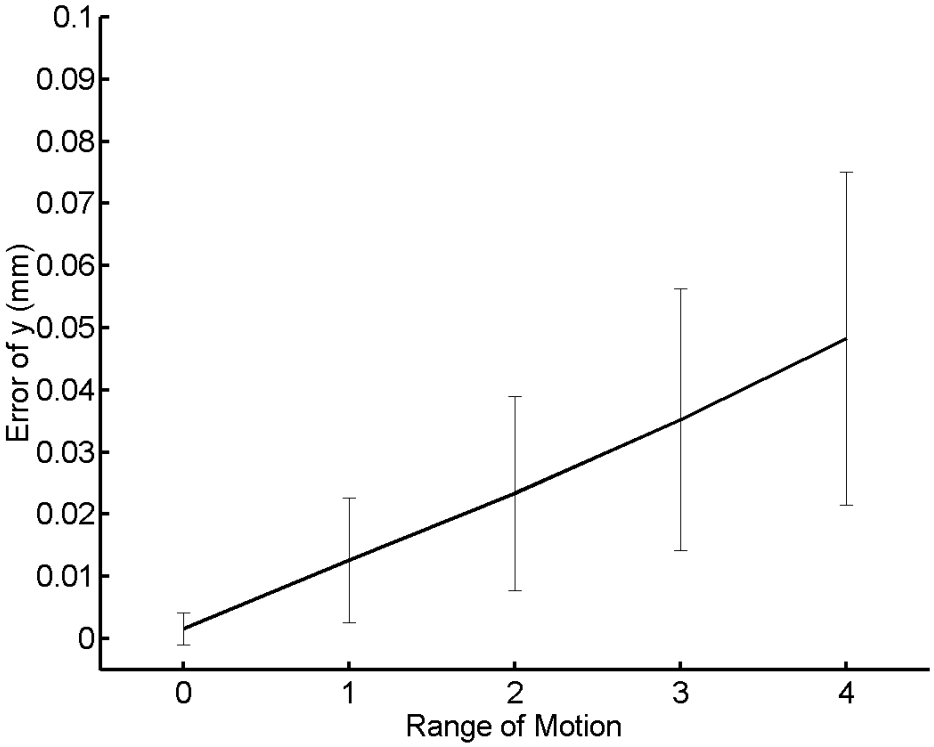

FIG. 7 Errors in elevational displacement estimation. The motion for all three rotation parameters ranges from 1 to 4°.

IV. EFFECTS OF COMPLEX MOTION ON ELEVATIONAL DISPLACEMENT ESTIMATION

Conventional methods estimate the elevational displacement without considering the other motion parameters. For freehand scanning, all six motion parameters are likely to exist. Figure 7 shows the effect of rotational motion on the error in y for a simulated y motion uniformly distributed between 0 and 0.08 mm. In other words, the average displacement is 0.04 mm and thus errors of 0.04 mm represent a 100% error. The horizontal axis of this figure is in degrees and it indicates the range of rotation for α, β and γ in degrees, where a range of 1 represents a variation of the three angles of between +/- 1°. The mean and the standard deviation of the estimated elevational displacement are shown. Likewise, results for the range of the three rotations at 2°, 3° and 4° are also shown. As the range of rotation increases, both the mean and the standard deviation increase. For each case, the mean and the standard deviation were calculated from at least 135 sets of images.

Figure 8 shows the elevational estimation errors when different types of errors are considered. Results of simple elevational motion (i.e., y only), elevational motion with in-plane rotation (i.e., y and α), elevational motion with in-plane rotation and one out-of-plane rotation (i.e., y, α and γ), and elevational motion with in-plane rotation and the two out-of-plane rotations (i.e., y, α, β and γ) are shown from (a) through (c) with the error bars representing +/- one standard deviation. As expected, the mean and the standard deviation increase when rotations are included.

Another effect influencing estimation accuracy is speckle variation. As shown in figures 5 and 6, the correlation distribution approaches to the final value only after the averaging of a

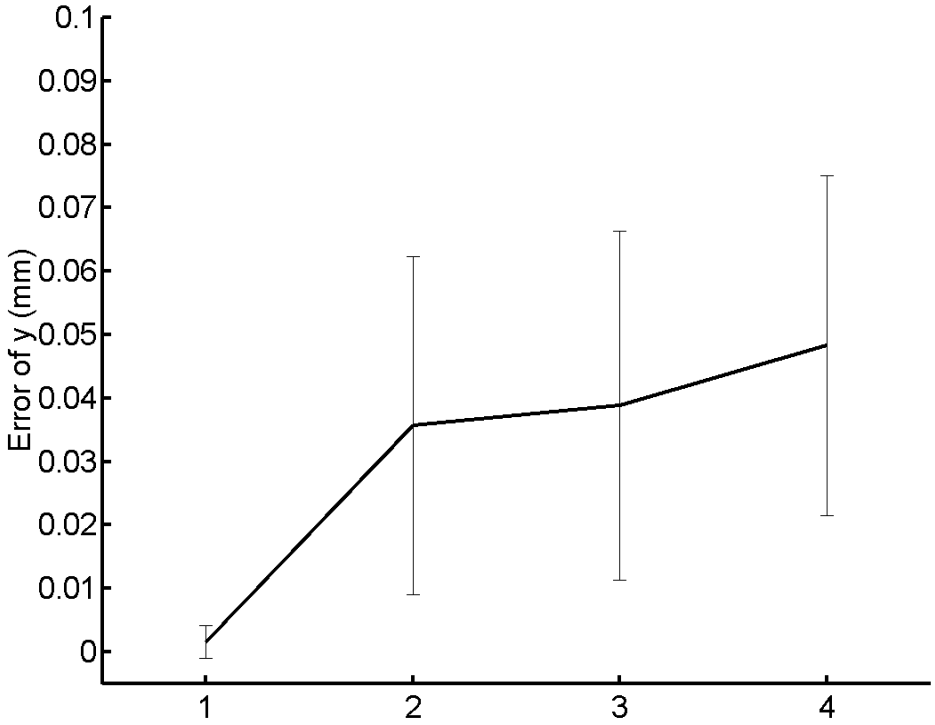

FIG. 8 Errors in elevational displacement estimation. The horizontal axis represents *y* and the included rotation parameters.

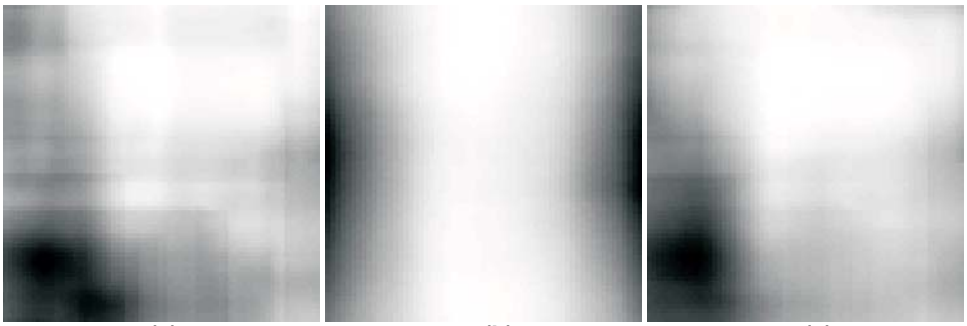

FIG. 9 Correlation distribution. (a: Single realization; (b) ensemble average; and (c) temporal average.

significant number of images (e.g., 10). However, this averaging is carried out on different realizations of the scatterer distribution (i.e., ensemble averaging), which is impossible in practice because there is only one scatterer distribution for a given image object. An alternative approach is to apply temporal averaging instead of ensemble averaging. The effectiveness of temporal averaging is shown in figure 9 using as an illustration a γ rotation of 4°. Figure 9(a) depicts the correlation distribution without averaging and (b) is the ensemble average of 20 realizations of the scatterer distribution. Ensemble averaging results in a reasonable correlation distribution, with the center vertical axis having the highest correlation and the correlation decreasing with lateral movement away from the center. Figure 9(c), on the other hand, shows the results of temporal averaging performed by averaging the correlation

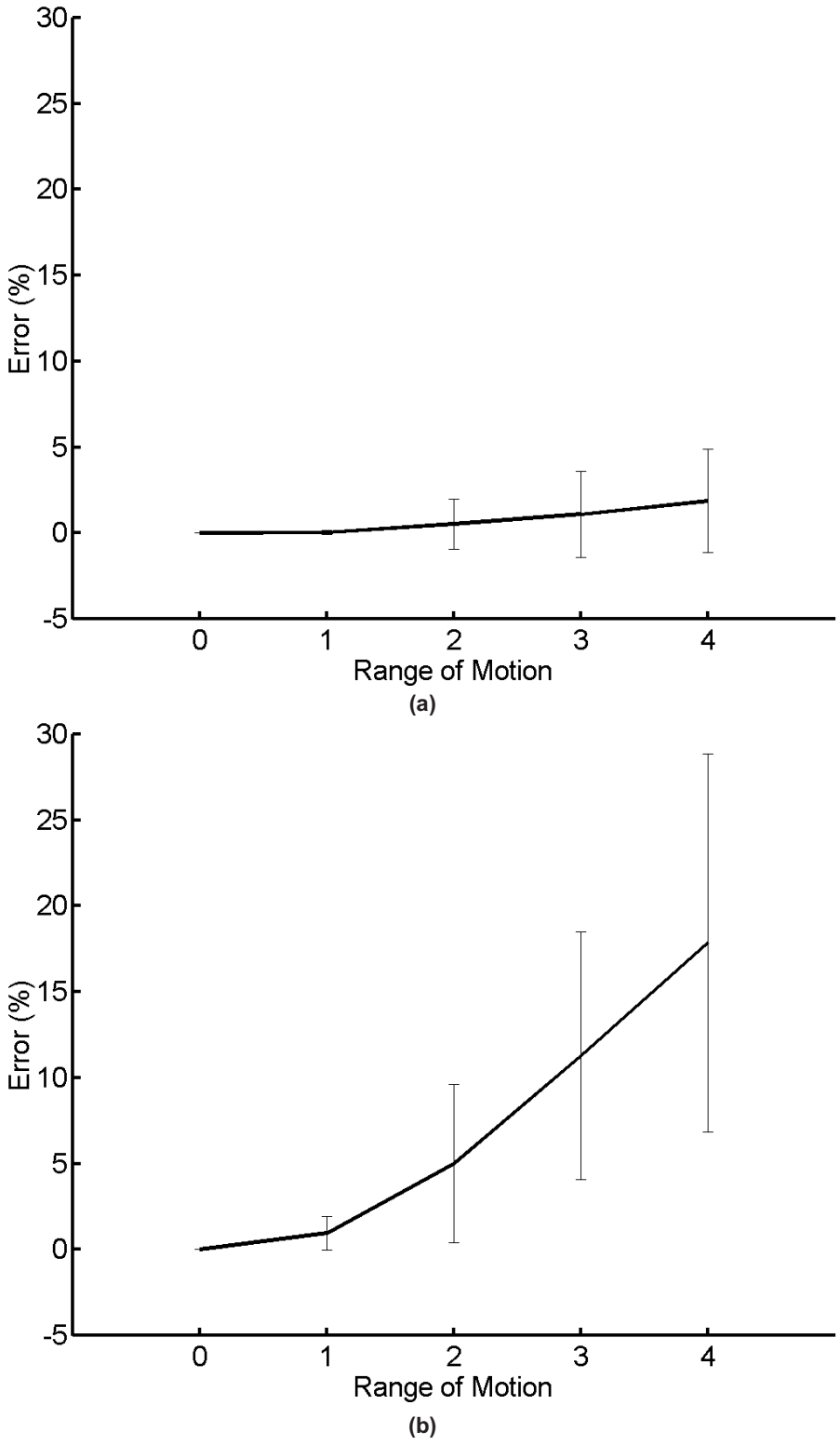

FIG. 10 Errors between the real correlation distribution and the product of the correlations of the simple motions. (a) *y* and γ; and (b) y, α, β and γ.

distributions acquired from consecutive image frames during a linear scan. It is clear that temporal averaging does not effectively reduce speckle variations. This is mainly due to the fact that the images are still obtained from the same 3D scatterer distribution. Additionally, in freehand scanning conditions the temporal averaging is performed on images that may have a random motion. Note that speckle variations can also be reduced by in-plane averaging. Nonetheless, the utility of in-plane speckle averaging is still limited because the number of independent correlation estimates for averaging may not be sufficiently large due to the size of the tracked region.

Finally, another potential problem with the application of correlation-based motion estimation is dependencies among the various motions. In the presence of complex motions, the correlation distribution cannot be approximated by some combination (e.g., product) of the individual correlations from the simple motions. This problem is illustrated in figure 10(a) and (b). Figure 10(a) shows the discrepancy between the real correlation distribution when both y and γ motions are present and the combined correlation approximated by the product of the individual y and γ correlations. In this figure, the vertical axis is the error in percentage and the horizontal axis is the range of motion, with 1 step representing 0.02 mm in y and 1° in γ. Figure 10(a) clearly shows that the discrepancy increases with the range of motion. This error further increases with the inclusion of more complex motions, as shown in figure 10(b) for a system in which y, α, β and γ motions are present.

V. CONCLUSION

In this paper, the effects of tissue motion on elevational displacement estimation were investigated. The results indicated that the estimation of elevational displacement may be significantly affected by rotational motion, even for rotations of only a few degrees. As shown in figures 7 and 8, the elevational estimation error can be as large as the average elevational displacement when the rotation is only 3°. T hus, such an effect cannot be ignored in clinical applications of freehand 3D if quantitative volume analysis is required. Furthermore, the elevational displacement is overestimated when speckle decorrelation from other motions is ignored. Thus, conventional approaches that do not consider other types of motion are not appropriate for freehand scanning. The results of the present work also showed that the elevational estimation accuracy is greatly improved if an external positioning device is used to estimate the out-of-plane rotation. This improvement arises because the in-plane motion estimation is relatively stable and the out-of-plane rotation parameters are obtained by the external device. Note that the advantage of such a hybrid approach is that, without sacrificing the positioning accuracy, it may be implemented at a cost lower than that of other methods that require a positioning device for full motion measurements (i.e., all six motion parameters). Finally, real freehand scanning without an external positioning device is still not possible. Although the correlation distribution throughout the image plane can be obtained, such a distribution is insufficient to find all the six motion parameters. As shown in this paper, the primary limitations are speckle variation and the fact that the correlation for complex motions cannot be derived from a combination of the correlations of simple motions.

REFERENCES

1. Nelson, T. R. and Pretorius, D. H., Three-dimensional ultrasound imaging, *Ultrasound Med. Biol. 24*, 1243-1270 (1998).

2. Light, E.D., Davidsen, R.E., Fiering, J.O., et al, Progress in two dimensional arrays for real time volumetric imaging, *Ultrasonic Imaging 20*, 1-16 (1998).

3. Barry, C.D., Allott, C.P., John, N.W., et al, Three-dimensional freehand ultrasound: Image reconstruction and volume analysis, *Ultrasound Med. Biol. 23*, 1209-1224 (1997).

4. Tuthill, T.A., Krucker, J.F., Flowlkes, J.B. et al, Automated three-dimensional US frame positioning computed from elevational speckle decorrelation, *Radiology 209*, 575-582 (1998).

5. Mo, L.Y.L., Hatfield, W.T. and Miller, S.C., Method and apparatus for tracking scan plane motion in free-hand three-dimensional ultrasound scanning using adaptive speckle correlation, *United States Patent*, 6, 012, 458 (2000).

6. Friemel, B. H., Weng, L. and Teo, T-J, 3-dimensional compound ultrasound filed of view, *United States Patent*, 5, 655, 535 (1997).

7. Li, M., System and method for 3-d medical imaging using 2-d scan data, *United States Patent*, 5, 582, 173 (1996).

8. Friemel, B.H., Weng, L., Teo, T-J, Brown, K.G., 3-dimensional volume by aggregating ultrasound fields of view, *United States Patent*, 5, 899, 861 (1999).

9. Li, P.-C., Cheng, C.-J. and Yeh, C.-K., On the velocity estimation using speckle decorrelation, *IEEE Trans. Ultrason. Ferroelect. Freq. Contr. 48*, 1084-1091 (2001).

10. Li, P.-C. and Chen, M.-J., Strain compounding: a new approach for speckle reduction, *IEEE Trans. Ultrason. Ferroelect. Freq. Contr. 49*, 39-46 (2002).

11. Kerr A. T. and Hunt, J. W., A method for computer simulation of ultrasound Doppler color flow images – II. Simulation results," *Ultrasound Med. Biol. 18*, 873–879 (1992).

12. Trahey, G. E., Allison, J.W. And von Ramm, O.T., Angle independent ultrasonic detection of blood flow, *IEEE Trans. Biomed. Eng., 34*, 965-967 (1987).

13. Trahey, G.E., Smith, S.W. and von Ramm, O.T., Speckle pattern correlation with lateral aperture translation: experimental results and implications for spatial compounding, *IEEE Trans. Ultrason., Ferroelect. Freq. Contr., 33*, 257-264 (1986).